JOURNAL OF MATERIALS SCIENCE 29 (1994) 4729–4735

Evaluation of the wettability of Al–Pb and Al–Sn alloys with SiC and Al_2O_3 particulates by means of pressure infiltration

A. ALONSO*, C. GARCIA-CORDOVILLA*, E. LOUIS*‡, J. NARCISO*, A. PAMIES*
** Industria Española del Aluminio, Centro de Investigación Y Desarrollo, Apartado 25, E-03080 Alicante, Spain*
‡ Departamento de Física Aplicada, Universidad de Alicante, Apartado 99, E-03080 Alicante, Spain

The wettability of SiC and Al_2O_3 particulates by Al–Pb and Al–Sn alloys has been evaluated by means of pressure infiltration. All infiltrations were carried out in air. The resulting threshold pressures decrease logarithmically with the content of the alloying element, similarly to the experimental data for the surface tension of these alloys reported in the literature. In the case of SiC, the threshold pressure decreases with the alloy content at a higher rate than the surface tension. In contrast, although the results for the alumina particulates are less clear, the tendency seems to be the opposite. These results are interpreted in terms of differences in wettability of silicon carbide and alumina particulates by oxidized aluminium–tin and aluminium–lead alloys.

1. Introduction

A major problem in the fabrication of aluminium–ceramic composites is the wettability of the reinforcement by the matrix [1]. Several engineering approaches have been adopted to improve wettability. They can be classified into two main groups [2]: (i) alloying additions that either promote reactions at the interface or modify the characteristics of the oxide layer that covers the surface of liquid aluminium, and (ii) coatings of the reinforcement that may react either with the metal matrix or with the oxide layer.

The evaluation of the performance of a method addressed to the improvement of wettability at metal–ceramic interfaces, usually requires a large amount of testing. There is therefore the need for a laboratory tool suitable for the evaluation of wettability. The standard method is the measurement of the contact angle [3, 4]. This measurement is not possible, however, when the solid is in the form of fibres, particulates or whiskers. Pressure infiltration may be an adequate tool in such cases [5]. In particular this method has been developed up to a rather convincing level for fibres [6–9]. In the case of particulates this development is still in its first stages [10–12].

In a previous paper [12] we investigated the applicability of laws that are known to govern a wide range of infiltration phenomena, such as Darcy's or capillary laws, to the infiltration of packed samples of ceramic particulates by liquid aluminium. The results were rather satisfactory [12]. In this work we study in detail the effect of surface tension on pressure infiltration, an issue that was also briefly considered earlier [12]. To this end we investigate the effects of lead and tin, two elements that are known to modify strongly the surface tension of pure aluminium, and that have been thoroughly investigated [13, 14]. Infiltrations were carried out on packed samples of alumina and silicon carbide particulates. The changes in the threshold pressures are compared to the changes in the surface tension of pure aluminium induced by Pb and Sn.

2. Experimental procedure

2.1. Materials

The alloys investigated in this work were prepared in alumina crucibles of 45 mm internal diameter × 72 mm height. Aluminium of commercial purity (approximately 99.98 wt %) was used throughout; typical amounts of impurities (wt %) are 0.015 Si and 0.005 Fe. Al–Pb and Al–Sn alloys were prepared from lead and tin of certificated purities 99.996 and 99.997%, respectively.

The characteristics of the Al_2O_3 and SiC particulates used in this work are summarized in Table I. The average diameters D of the particulates were determined by laser light scattering using a Malvern Mastersizer. The indices of refraction of silicon carbide and alumina particulates used in these determinations were 2.67 and 1.7, respectively. The average diameter and the span of the size distribution are given in Table I. Scanning electron microscope (SEM) micrographs of the two particulates are shown in Fig. 1. SiC particulates have a non-spherical angular shape, whereas alumina particulates are in the form of platelets. Although a thorough characterization of the

0022–2461

TABLE I Characteristics of the SiC (99.5%) and Al_2O_3 (99.0%) particulates used in this work

	Type/shape	Purity	Average particulate diameter, D (μm)	Span[a]	Particle volume fraction, V_p	$V_p/[D(1 - V_p)]$
SiC	green	99.5%	26	0.8	0.57	0.0510
Al_2O_3	platelets	99.0%	18	1.1	0.58	0.0767

[a] Given by $[D(90) - D(10)]/D(50)$, where $D(10)$, $D(50)$ and $D(90)$ are the diameters below which 10, 50 and 90%, respectively, of the particles are found.

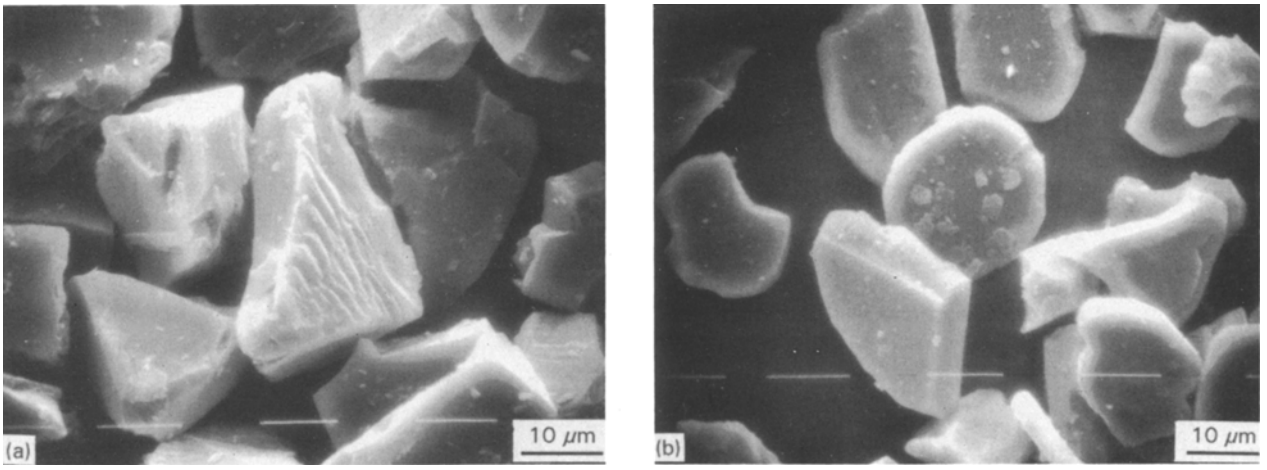

Figure 1 Scanning electron micrographs of (a) SiC and (b) Al_2O_3 particulates used in this work.

surface condition of the particulates would require a detailed study [15], SEM micrographs clearly indicate that their surfaces are apparently free of residues.

2.2. Experimental apparatus and procedures

The infiltration experiments were carried out in a pressure chamber that was described in detail earlier [12]. Here we shall only outline its main features. It was made of stainless steel, and could support a maximum pressure of 3000 kPa. A resistance furnace was located inside the chamber. Pressure was measured with a transmitter and controlled within $\pm$ 2 kPa. Pressure and temperature were registered during the whole experiment. All pressures are referred to atmospheric pressure.

The particulates were packed into quartz tubes of 5 mm i.d. × 20 cm length. At each packing step, approximately 0.04 g of particulates were added, followed by 3 s of vibrations to break layering, and the powder was subjected to 20 strokes of a 35 g weight from a constant height (10 cm). The procedure was repeated until the compact reached a height of $\sim$ 3.5 cm. In order to determine the particle volume fraction V_p the quartz tube was weighed before and after the powder was packed inside it, and its diameter measured at five points along its perimeter. Measurements of the length of the packed powder then allowed one to obtain V_p. The densities of the alumina and silicon carbide particulates used in these determinations were 3.9 an 3.21 g cm^{-3}, respectively. The melt side of the compact was plugged with alumina paper with 6% of theoretical density, to avoid depacking and to skim off the alumina scum during infiltration. A ceramic rod was placed on the top of the preforms to prevent them from moving upwards in the quartz tube during infiltration.

The infiltrations were carried out at a melt temperature of 750 $\pm$ 2 °C. The metal surface was cleaned just before the immersion of the quartz tube containing the packed specimens. As no inert gas was introduced into the packed powder it is expected that, along the whole infiltration process, a thin oxide layer will cover the surface of the aluminium. The chamber was closed and the tube held in the melt for 3 min. Pressure was then applied with nitrogen gas at a rate of 50–60 kPa s^{-1}, up to the chosen pressure. After a fixed period of time (120 s in the present work) the chamber was vented at a rate of 30–70 kPa s^{-1}. The sample was taken out of the melt and air-cooled; it was then sectioned and the infiltration height measured with a precision gauge.

2.3. Chemical compositions and metallography

The chemical composition of the alloys after infiltration was determined by means of atomic absorption spectroscopy. Samples were taken from the aluminium side of the tubes (unreinforced portions of the castings). As noted elsewhere [12], it was found that the silicon content was raised to 0.35 wt %, due to the reaction of aluminium with the quartz tubes. This is not a serious problem, however, as the changes in the surface tension of pure aluminium promoted by silicon are comparatively very small [16].

The infiltrated samples were sectioned, mounted in bakelite and polished on an automatic polisher to

show the microstructure of the composite. A first grinding was achieved by means of SiC carbide papers with grits in the range 240–1200. The intermediate stages consisted of polishing with diamond paste (15 and 6 μm) on Metcloth. The final polish was performed with colloidal silica on Microcloth. The microstructure was studied by means of optical microscopy, scanning electron microscopy and energy-dispersive X-ray analysis (EDAX).

3. Results

3.1. Infiltration

The results for the infiltrated height versus applied pressure are reported in Figs 2 and 3. In most cases, at least eight different infiltration experiments were required to localize the relevant pressure range for each composition. For some compositions further infiltrations were needed to check the results. For instance, this is the case for alumina particulates infiltrated with the alloy containing 0.5 wt % Pb. The reproducibility was in all cases satisfactory. A total of around 100 samples were infiltrated. The infiltrated samples containing alumina could be easily broken into small pieces, indicating that, in these samples, bonding at the metal–ceramic interface was poor (see below).

3.2. Microstructure of the infiltrated samples

The optical micrograph of Fig. 4 shows three differentiated regions, namely the alloy, the infiltrated alumina paper and the composite. The porosity is normal for this kind of sample [12]. We only show micrographs of an Al–Sn alloy, as the maximum lead content used in this work is too low to facilitate the observation of the microstructure. Note, however, that

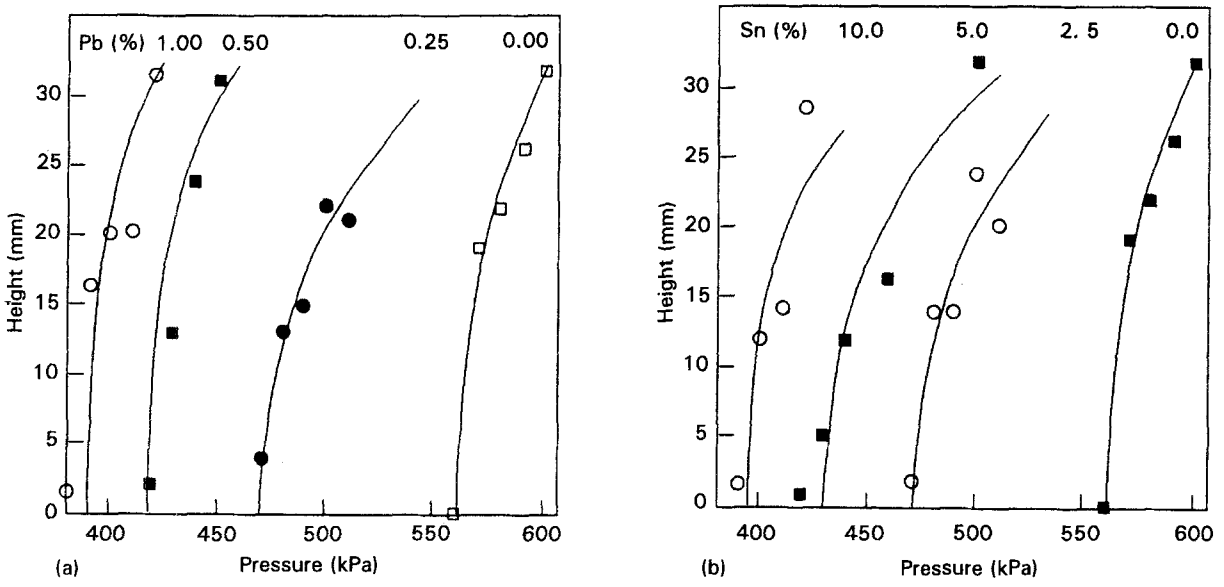

Figure 2 Infiltrated height as a function of applied pressure (infiltration time, 120 s; $T = 750\,^{\circ}C$) for packed samples of the SiC particulates of Table I infiltrated with (a) Al–Pb alloys (0–1 wt % Pb) and (b) Al–Sn alloys (0–10 wt % Sn).

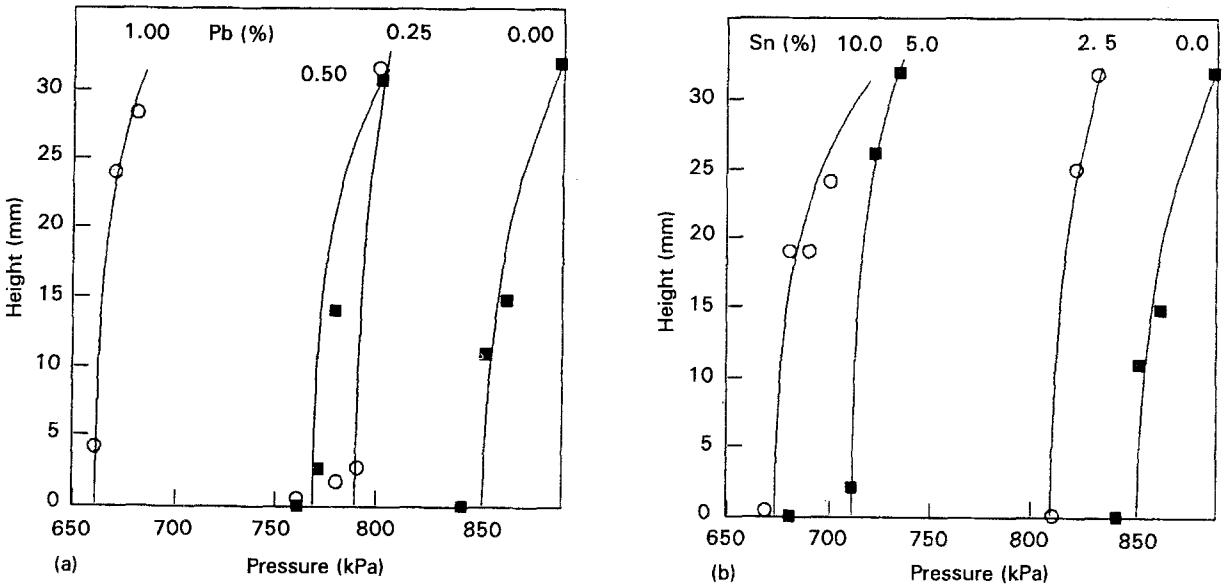

Figure 3 Infiltrated height as a function of applied pressure (infiltration time, 120 s; $T = 750\,^{\circ}C$) for packed samples of the Al_2O_3 particulates of Table I infiltrated with (a) Al–Pb alloys (0–1 wt % Pb) and (b) Al–Sn alloys (0–10 wt % Sn).

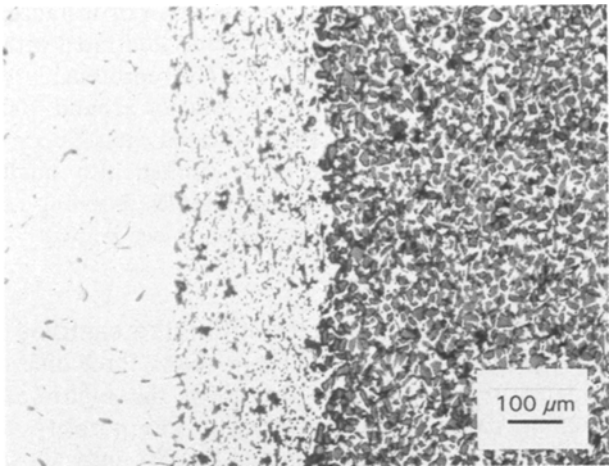

Figure 4 Microstructure of a packed sample of SiC particulates infiltrated with an Al–5 wt% Sn alloy. Three regions are clearly differentiated, namely the alloy, the infiltrated alumina paper and the infiltrated particulate compact.

as neither of the two elements form intermetallics with aluminium, the microstructures of the two alloys are very alike, i.e. pure aluminium and pure tin (or lead) mainly localized in the interdendritic spaces. In the composite, both lead and tin are preferentially localized close to the ceramic particles. This is clearly illustrated in Fig. 5, where an EDAX mapping allows one to identify the tin particles.

4. Discussion

4.1. Determination of threshold pressures

The threshold pressure for infiltration can be determined from the data reported in Figs 2 and 3. This could be done by assuming that flow of liquid aluminium through the packed samples of alumina or silicon carbide particulates is governed by Darcy's law [5]. For unidirectional flow and neglecting any effect of gravity, Darcy's law can be written as

$$h = \left(\frac{2kt\Delta P}{\mu(1 - V_p)}\right)^{1/2} \quad (1)$$

where ΔP is the pressure drop in the liquid metal, given by the difference between the total pressure drop that can be identified with the applied pressure P and the threshold pressure P_0, namely $\Delta P = P - P_0$.

Darcy's law is known to be valid under the following conditions [5, 6]: (i) a sharp infiltration front, (ii) finite infiltration times, and (iii) Reynolds numbers smaller than 1. The first is an important objection only for results concerning small infiltration heights which, as discussed elsewhere [12], may also be affected by other experimental factors. The second point does not apply to the present experiments as the infiltration time chosen in this work is rather high (120 s). Finally, the third point can be checked by estimating the Reynolds number Re, which is given by the expression

$$Re = \frac{D\rho_m v_0}{\mu V_p} \quad (2)$$

where ρ_m is the density of the liquid metal and v_0 the superficial velocity of the fluid. Introducing the highest superficial velocity achieved in the present experiments ($\sim 0.25 \times 10^{-3}$ m s^{-1}), the viscosity of pure aluminium (1.06 mN s m^{-2}) and the data of Table I into Equation 2, we obtain 0.017 and 0.025 for alumina and silicon carbide particulates, respectively. These values of the Reynolds number are small enough to expect Darcy's law to be valid in the infiltrations carried out in this work. Similarly small values of Re are obtained for all the particulates considered earlier [12].

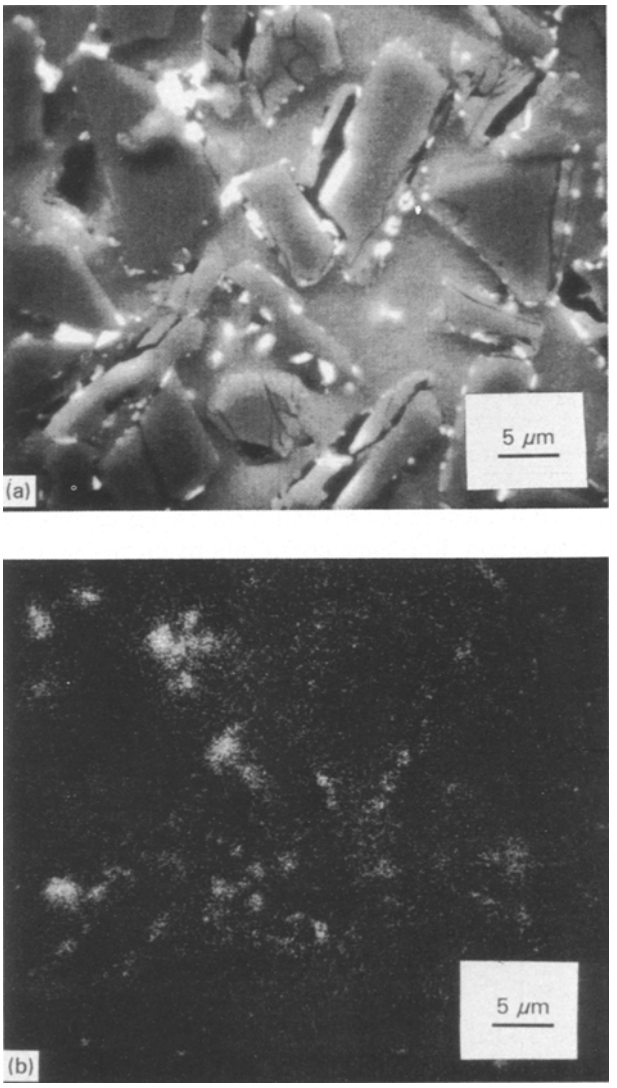

Figure 5 SEM micrograph of a packed sample of Al_2O_3 particulates infiltrated with an Al–5 wt % Sn alloy; (b) EDAX mapping of Sn in the same sample, which clearly shows that the bright spots in (a) are tin particles.

Thus we expect that a determination of the threshold pressures through a fitting of the experimental data of Figs 2 and 3 by means of Equation 1 should be accurate enough. Our previous analysis [12] gives further support to this procedure. The fitted curve is

$$P = ah^2 + b \quad (3)$$

where a and b are constants, and the latter gives the threshold pressure. The fitted curves and the corresponding regression coefficients are reported in Table II. The experiments that gave very small values of the infiltrated height at pressures below threshold (estimated by extrapolating the data to zero infiltration

TABLE II Curves fitted to the experimental results for infiltrated height as a function of applied pressure: $P = ah^2 + P_0$, where P_0 is the threshold pressure; the regression coefficients r of the fittings are also given

Metal		Al_2O_3		SiC	
Alloy	wt %	$P(h)$(kPa)	r	$P(h)$(kPa)	r
Al	99.9	$0.039\,h^2 + 853$	0.95	$0.041\,h^2 + 559$	0.99
Al–Pb	0.25	–	–	$0.077\,h^2 + 470$	0.95
	0.5	$0.055\,h^2 + 766$	0.97	$0.030\,h^2 + 422$	0.99
	1.0	$0.024\,h^2 + 659$	0.97	$0.033\,h^2 + 385$	0.90
Al–Sn	2.5	–	–	$0.061\,h^2 + 473$	0.85
	5.0	–	–	$0.066\,h^2 + 439$	0.90
	10.0	$0.041\,h^2 + 671$	0.97	$0.034\,h^2 + 396$	0.90

height) were not included in the fittings, as done previously [12]. In three cases a reliable fitting of the results was not possible due to the fast rise of the infiltrated height as a function of applied pressure. In such cases threshold pressures were estimated by extrapolation of the experimental data to zero infiltration height.

4.2. The capillary law

The threshold pressure P_0 for infiltration is related to the surface tension of the infiltrating liquid through the so-called capillary law [4, 10]

$$P_0 = 6\lambda\,\gamma_{lv}\cos\theta\frac{V_p}{(1 - V_p)D} \quad (4)$$

where γ_{lv} is the liquid–vapour surface tension, θ the contact angle and λ a factor which depends on the geometry of the particulates. D and V_p are the mean diameter and volume fraction of the particulate, respectively, given in Table I.

In our previous work [12] we showed that P_0 decreases as $1/D$, in agreement with Equation 4. The experimental results for the threshold pressure reported in Table II show that it decreases with the lead or tin content and, consequently, with the surface tension of the alloy (note that both additions reduce the surface tension of pure aluminium [13, 14]). This is in qualitative agreement with the capillary law. In order to quantify this result we have first fitted the experimental data for the relative change in the surface tension of these alloys, $[\gamma_{lv}(x) - \gamma_{lv}(0)]/\gamma_{lv}(0)$, in the compositional range here considered by means of the curve [14]

$$f(x) = a\ln(1 + bx) \quad (5)$$

where x (wt %) is the alloying element content. The fitted curves are reported in Table III and shown in Figs 6 and 7. Similar fittings have been carried out of the experimental data for the relative change in the threshold pressure, $[P_0(x) - P_0(0)]/P_0(0)$, as a function of the alloy content x. The results are also shown in Table III and Figs 6 and 7. The fits for silicon carbide particulates are very good, but those for alumina are rather poor.

The trend of the results shown in Figs 6 and 7 qualitatively supports the capillary law, namely the threshold pressure decreases with the surface tension of the alloy. However, it is noted that, in the case of SiC, the threshold pressure decreases with the alloy content faster than the surface tension of the alloy. On the other hand, in the case of alumina particulates

TABLE III Curves fitted to the experimental results for the threshold pressure $P_0(x)$ as a function of the content of the alloying element x (wt %), together with curves fitted to the data for the surface tension $\gamma_{lv}(x)$ reported earlier [14]; the fittings were carried out for x in the ranges investigated in this work (see Table II) and $T = 750\,^\circ C$

Alloy	$\gamma_{lv}(x) - \gamma_{lv}(0)$ (mN m^{-1})	$P_0(x) - P_0(0)$(kPa)	
		Al_2O_3	SiC
Al–Pb	$-107\ln(1 + 5.83\,x)$	$-5510\ln(1 + 0.035\,x)$	$-73\ln(1 + 10\,x)$
Al–Sn	$-84\ln(1 + 0.67\,x)$	$-225\ln(1 + 0.13\,x)$	$-67\ln(1 + 1.0\,x)$

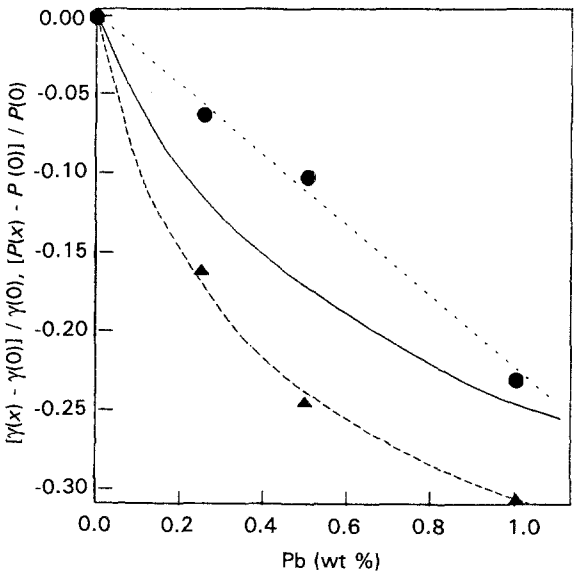

Figure 6 Relative change in the threshold pressure, $[P_0(x) - P_0(0)]/P_0(0)$, required to infiltrate packed samples of (▲) SiC and (●) Al_2O_3 particulates with Al–Pb alloys as a function of the content x of the alloying element. The relative change in the surface tension, $[\gamma_{lv}(x) - \gamma_{lv}(0)]/\gamma_{lv}(0)$, as reported by Goumiri *et al.* [14], are also given (——). The fitted curves (– – – – – –) are reported in Table V. Infiltration conditions: infiltration time 120 s and $T = 750\,^\circ C$.

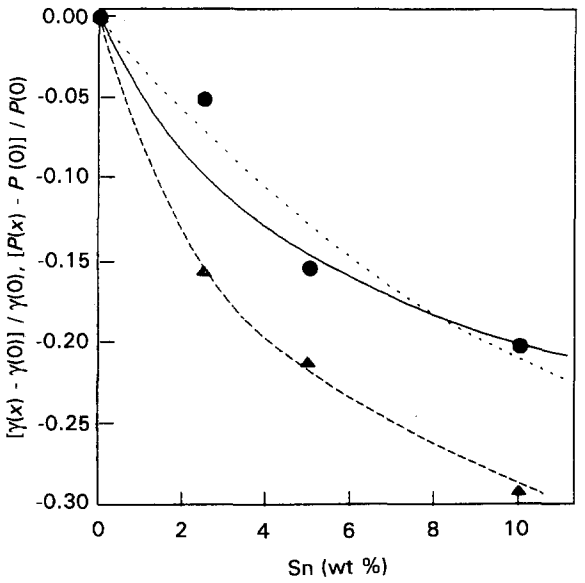

Figure 7 Relative change in the threshold pressure, $[P_0(x) - P_0(0)]/P_0(0)$ required to infiltrate packed samples of (▲) SiC and (●) Al_2O_3 particulates with Al–Sn alloys as a function of the content of the alloying element. The relative change in the surface tension, $[\gamma_{lv}(x) - \gamma_{lv}(0)]/\gamma_{lv}(0)$, as reported by Goumiri *et al.* [14], are also given (——). The fitted curves (– – – – – –) are reported in Table V. Infiltration conditions: infiltration time 120 s and $T = 750\,°C$.

TABLE IV Threshold pressures P_0 (kPa) for infiltration at $T = 750\,°C$, for Al–Pb alloys; γ_{lv} is the surface tension of the liquid metal reported earlier [12] and A gives $\cos\theta_{alloy}/\cos\theta_{Al}$ (see Equations 6 and 7)

Metal		Al_2O_3		SiC	
Pb (wt %)	γ_{lv} (mN m^{-1})	P_0 (kPa)	A	P_0 (kPa)	A
0	854	853	1.0	559	1.0
0.25	758	800	1.057	470	0.948
0.5	708	766	1.083	422	0.911
1.0	648	659	1.018	385	0.908

TABLE V Threshold pressures P_0 for infiltration at $T = 750\,°C$, for Al–Sn alloys; γ_{lv} is the surface tension of the liquid metal reported earlier [12] and A gives $\cos\theta_{alloy}/\cos\theta_{Al}$ (see Equations 6 and 7)

Metal		Al_2O_3		SiC	
Sn (wt %)	γ_{lv} (mN m^{-1})	P_0 (kPa)	A	P_0 (kPa)	A
0	854	853	1.0	559	1.0
2.5	772	810	1.051	473	0.927
5	731	720	0.985	439	0.917
10	683	671	0.985	396	0.886

most of the results show the opposite tendency, although in some cases the relative change in P_0 is almost the same as the relative change in the surface tension. These differences between alumina and silicon carbide particulates may be a consequence of differences in wetting, and will be further considered in the next subsection.

4.3. Contact angles

Assuming that the capillary law (Equation 4) is valid, the deviations from this law discussed in the previous subsection should be ascribed to changes in the contact angle. These can be estimated in the following way. For a given particulate, and applying the capillary law to pure aluminium and a particular aluminium alloy, we can eliminate the geometric factor λ and obtain an expression for the contact angle of the alloy

$$\cos\theta_{alloy} = A\cos\theta_{Al} \quad (6)$$

where A is given by

$$A = \frac{\gamma_{Al}}{\gamma_{alloy}}\left(\frac{P_0^{alloy}}{P_0^{Al}}\right) \quad (7)$$

Equations 6 and 7 relate the contact angle for a given aluminium alloy (θ_{alloy}) to the contact angle of pure aluminium (θ_{Al}), and the corresponding threshold pressures and liquid–vapour surface tensions. Note that Equation 6 is only valid for a set of experimental data corresponding to the same particulate, and therefore for constant D, V_p and λ. The results for A (Equation 6) are reported in Tables IV and V. These results, which are nothing but a different form of presenting the data of Figs 6 and 7, clearly indicate that in the case of SiC, both tin and lead increase wetting, in agreement with the earlier result [12] for an Al–1 wt % Pb alloy. The results for alumina are less clear although the tendency is the opposite, namely a decrease in wetting.

In translating these results into specific changes in the contact angles, it should be first decided which experimental data for the contact angle of pure aluminium are applicable in the present experimental conditions. According to Laurent *et al.* [3] the most adequate contact angle between aluminium and SiC for short-time contacts, temperatures below 1000 K, and removing the oxide layer that covers liquid aluminium by mechanical pressure, is $120 \pm 5°$. In the case of alumina [17, 18] the relevant contact angle for oxidized aluminium is slightly smaller, i.e. $109 \pm 6°$. At high temperatures the oxide layer that covers aluminium is removed and the metal wets both ceramics. It should be noted that these contact angles were measured on polished monocrystals. Furthermore, impurities and the different roughness of the present SiC particulates can alter this angle. Thus, although the values for the contact angle given above are probably valid for the present experiments, these considerations motivated our decision to present the results as relative changes in θ (see Tables IV and V). However, some estimations of the contact angle can be made. For example, if we take for the contact angles at the Al–SiC and Al–Al_2O_3 interfaces the values given above (120 and 109°, respectively), the results of Tables IV and V give 116.3 and 108.7°, respectively, for the Al–10 wt % Sn alloy and 117 and 109.4°, respectively, for the Al–1 wt % Pb alloy.

These results cannot be easily interpreted. On the one hand, contact angle measurements indicate that both pure tin and lead do not wet the two ceramics

investigated here [17–20]; tin additions seem to slightly decrease the contact angle at the unoxidized Al–alumina interface [18]. Thus, available contact angle data are not compatible with the present results. On the other hand the results cannot be understood in terms of a weakening or disruption of the oxide layer that covers aluminium, because in such a case the wetting had increased for the two ceramics. The only possibility is the *ad hoc* assumption that tin and lead modify the characteristics of the oxide layer (in particular its chemistry) in such a way as to favour wetting of SiC.

5. Concluding remarks

In this paper we have presented the results of an investigation of the effects of surface-active additions on pressure infiltration of packed samples of two ceramic particulates (SiC and Al_2O_3) by liquid aluminium. In particular we have shown that both lead and tin additions decrease the threshold pressure for infiltration. The reduction in the threshold pressure is mainly a consequence of a corresponding decrease in the surface tension promoted by both elements. On the other hand, the results for SiC do further suggest that both tin and lead increase wetting at the aluminium–SiC interface. Although the experimental data for alumina are less clear, the tendency seems to be the opposite. These results can only be understood by assuming that lead and tin additions modify the characteristics of the oxide layer so as to increase wetting at the aluminium–SiC interface.

The present results give further support to pressure infiltration as a reliable and efficient tool in the evaluation of wettability between liquid metals and ceramic particualtes. Recent studies of the effect of the morphology and surface condition of the particulates, and of coating designed to react with the oxide layer [21], point in the same direction.

Acknowledgements

The authors are grateful to the Industria Española del Alumino for permission to publish this work. Financial support from the Centro para el Desarrollo Tecnológico Industrial (contract P-10117), the ministerio de Industria, Comercio y Turismo (contract 171/92), the Instituto Nacional de Industria (contract H-199), and the commission of the European Communities (Science Programme, contract SC1-0384-C(A)) is gratefully acknowledged. A Alonso and J. Narciso are also grateful to the Ministerio de Educatión y Ciencia for financial support.

References

1. D. J. LLOYD, in "Advanced Structural Materials", edited by D. S. Wilkinson (Pergamon, London, 1989) p. 1.
2. A. MORTENSEN and I. JIN, *Int. Metall. Rev.* **235** (1992) 101.
3. V. LAURENT, D. CHATAIN and N. EUSTATHOPOULOS, *J. Mater. Sci.* **22** (1987) 244.
4. F. DELANNAY, L. FROYEN and A. DERUYTTERE, *J. Mater. Sci.* **22** (1987) 1.
5. J. BEAR, "Dynamics of fluids in porous media" (Dover, New York, 1988) pp. 161–176.
6. A. MORTENSEN, L. J. MASUR, J. A. CORNIE and M. C. FLEMINGS, *Metall. Trans.* **20A** (1989) 2535.
7. J. L. MASUR, A. MORTENSEN, J. A. CORNIE and M. C. FLEMINGS, *ibid.* **20A** (1989) 2549.
8. A. MORTENSEN and V. J. MICHAUD, *ibid.* **21A** (1990) 2059.
9. V. J. MICHAUD and A. MORTENSEN, *ibid.* **23A** (1992) 2263.
10. S. Y. OH, J. A. CORNIE and K. C. RUSELL, *ibid.* **20A** (1987) 527.
11. J. GOICOECHEA, C. GARCÍA-CORDOVILLA, E. LOUIS and A. PAMIES, in "Composite Materials", edited by A. T. Di Benedetto, L. Nicolais and R. Watanabe (North Holland, Amsterdam, 1992) p. 221.
12. A. ALONSO, A. PAMIES, J. NARCISO, C. GARCÍA-CORDOVILLA and E. LOUIS, *Metall. Trans.* **24A** (1993) 1423.
13. G. LANG, *Aluminium* **50** (1974) 731.
14. J. GOUMIRI, J. C. JOUD, P. DESRE and J. M. HICTER, *Surf. Sci.* **83** (1979) 471.
15. J. NARCISO, C. GARCÍA-CORDOVILLA and E. LOUIS, *Mater. Sci. Engng* **B15** (1992) 148.
16. J. GOICOECHEA, C. GARCÍA-CORDOVILLA, E. LOUIS and A. PAMIES, *J. Mater. Sci.* **27** (1992) 5247.
17. L. COUDURIER, J. ADORIAN, D. PIQUE and N. EUSTATHOPOULOS, *Rev. Int. Tempér. Réfract.* **21** (1984) 81.
18. J. G. LI, D. CHATAIN, L. COUDURIER and N. EUSTATHOPOULOS, *J. Mater. Sci. Lett.* **7** (1988) 961.
19. JU, V. NAIDICH, *Progr. Surf. Membr. Sci.* **14** (1981) 353.
20. I. RIVOLLET, Thése INPG, Grenoble (1986).
21. A. ALONSO, J. NARCISO, A. PAMIES, C. GARCÍA-CORDOVILLA and E. LOUIS, *Scripta Metall. Mater.* **29** (1993) 1559.

Received 29 July 1993
and accepted 19 January 1994